

Aerodynamic Shape Design of the Vertical Landing Rocket Vehicle

Yoshinori Namera¹

Tokyo University of Science, Chiyoda, Tokyo, 102-0073, Japan

Ryoji Takaki², Akira Oyama³, Kozo Fujii⁴

Institute of Space and Astronautical Science of JAXA, Sagami-hara, Kanagawa 252-5210 Japan

and

Makoto Yamamoto⁵

Tokyo University of Science, Chiyoda, Tokyo, 102-0073 Japan

Aerodynamic characteristics of a vertical landing rocket vehicle are computationally investigated under subsonic and supersonic flight conditions as a preliminary study for the concept design using a light optimization method and a light CFD tool. The results show that the simulations with a coarse grid can accurately estimate the aerodynamic characteristics like axial force coefficient and the lift-to-drag ratio. The results of the light aerodynamic shape optimization indicate tradeoff information among objective functions, and the correlation between design variables and objective functions. The preliminary knowledge for the aerodynamic shape design is obtained.

Nomenclature

C_A	= Axial force coefficient, axial force / $(q_\infty S_{ref})$
C_D	= Drag coefficient, drag / $(q_\infty S_{ref})$
C_L	= Lift coefficient, lift / $(q_\infty S_{ref})$
L/D	= Lift-to-drag ratio
M_∞	= Free stream Mach number
q	= Dynamic pressure
Re	= Free stream Reynolds number based on the base diameter of the body
S_{ref}	= Reference area
θ_{kin}	= Kink angle of the body geometry
θ_r	= Aft body angle of the body geometry

I. Introduction

THE vertical landing reusable rocket vehicle has been proposed as one of the future space transportation systems. It is considered to have a greater advantage than other space transportation systems because the vehicle does not need any massive ground supporting systems and more effective ground operations are expected. Institute of Space and Astronautical Science of Japan Aerospace Exploration Agency (ISAS/JAXA) has been developing a reusable sounding rocket vehicle,¹ which can lift off and land vertically and reach to the altitude of 120 km. The compact Reusable Vehicle Testing (RVT) has been conducted having many experiments about liftoff and landing (Fig. 1).

¹ Graduate Student, Department of Mechanical Engineering, kudankita 1-14-6, Currently Central Japan Railway Company.

² Associate Professor, Department of Space Science Information Analysis, 3-1-1, Yoshinodai and Member AIAA.

³ Associate Professor, Department of Space Transportation Engineering, 3-1-1, Yoshinodai and Member AIAA.

⁴ Professor, Department of Space Transportation Engineering, 3-1-1, Yoshinodai and Fellow AIAA

⁵ Professor, Department of Mechanical Engineering, 1-14-6, Chiyoda and Member AIAA.

It is necessary to have a certain downrange during the return phase for the safety flight, as well as minimize the aerodynamic drag during the ascent phase for the liftoff capability in the system design of the reusable sounding rocket vehicle. Therefore, the nose-entry and base-landing is considered as the flight sequence and adoption of a slender body shape and aileron is discussed. Figure 2 shows the planned sequence of the flight.

The aerodynamic shape design of the vehicle is indispensable to meet the design requirements, mentioned above. The ascent altitude and the downrange of the vehicle were estimated by the conventional preliminary design tools.¹ The estimated results and succeeded studies show the difficulties to realize the design requirements. The aerodynamic characteristics for several body configurations of the vehicle were not sufficiently discussed so far. It is important for the aerodynamic design to learn about the aerodynamic characteristics in various flight conditions because the reusable sounding rocket vehicle has a greatly different body configuration from the conventional space transportation vehicles and it flies at a wide range of the flight speed and attack angles. Computational Fluid Dynamics (CFD) is suitable to use at conceptual design stage of the aerodynamic configurations as it is able to get aerodynamic characteristics from more configurations than wind tunnel testing.

The objective of the paper is to understand the aerodynamic characteristics for various body configurations by using the advantage of CFD in order to have knowledge for the aerodynamic shape design of the reusable sounding rocket vehicle, which is currently under development at ISAS/JAXA. For this purpose, multi-objective design explorations for the aerodynamic configuration are conducted by using CFD to minimize the aerodynamic drag during the ascent phase, to maximize the maximum lift-to-drag ratio during the return phase and to maximize the body volume. The obtained results are discussed to have knowledge required for the preliminary aerodynamic configuration design.

II. Definition of the Design Problem

The design requirements for the vehicle are that the ascent altitude is more than 120 km and the downrange during the return phase is more than 30 km, which are difficult to have been achieved by the studies so far. In this study, multi-objective design exploration for the aerodynamic configuration is conducted by using CFD. The aerodynamic drag during the launch has a great impact on the ascent altitude. It is mainly affected around the maximum dynamic pressure region, where Mach number is 2.0 and attack angle is 0 degree. The maximum lift-to-drag ratio during the return phase has a great impact on the downrange. There are two flight regions to be considered for the maximum lift-to-drag ratio. One is a subsonic flight region whose Mach number is 0.8 and the other is a supersonic flight region whose Mach number is 2.0. The aerodynamic characteristics of the subsonic and supersonic flight regions are greatly different from each other. Therefore, both flight regions should be addressed to consider the maximum lift-to-drag ratio. The maximization of the body volume is also necessary in order to enlarge on-board capability for payloads, fuel and equipments.

The objective functions so far mentioned are summarized as follows.

The objective function 1: the drag minimization at 2.0 of Mach number and 0 degree of the attack angle.

The objective function 2: the maximum lift-to-drag ratio maximization at 0.8 of Mach number.

The objective function 3: the maximum lift-to-drag ratio maximization at 2.0 of Mach number.



Figure 1. Reusable Vehicle Testing (RVT)

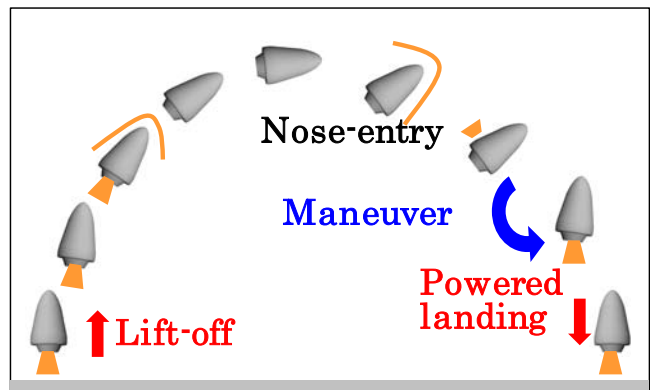


Figure 2. Flight sequence (nose-entry and base-landing)

The objective function 4: the body volume maximization.

The vehicle body is axisymmetric shape and has one kink. Figure 3 shows the body geometry. The base diameter and the length of the vehicle body are 3 m and 10 m, respectively. The slenderness ratio is 3.33. These are the same geometry of the reusable sounding rocket currently under development at ISAS/JAXA. The lengths in the figure are non-dimensionalized by the base diameter. The design variable used in this study is the position of the kink, which are represented by the kink angle θ_{kin} and the angle of the aft body after the kink θ_r , shown in Fig. 3. The body geometry is changed by the position of the kink, namely θ_{kin} and θ_r . Other body configuration parameters such as a nose radius (rf), a base corner radius (R) and a base radius (rs) are fixed in this study, also shown in Fig. 3. It is shown in Ref. 2 that these fixed parameters have a small impact on the current objectives or they are difficult to be evaluated by the numerical method used in this paper. Especially, it is known that the base radius and the base corner radius have a large impact on the aerodynamic characteristics. However, computationally expensive method like LES is required to estimate the effect of these parameters precisely. In this paper, computationally inexpensive method like RANS simulation is used because the aim of the paper is to obtain the valuable knowledge required at the conceptual aerodynamic design stage. Therefore, these parameters are fixed in this study.

The grid search method is used to explore the design variable space because the number of design variables is small (only two) and this paper aims not to get the optimized body geometry but the overview of the design variable space. The total number of the body configuration studied in this work is 27. The exploration area of the design variables is shown in Fig. 4. The angle of attack and the aerodynamic coefficients (C_A , C_L and C_D) are defined, respectively as shown in Fig. 5. The aerodynamic drag and the lift-to-drag ratio are defined as C_A and C_L/C_D , respectively. As for the supersonic case, the maximum lift-to-drag ratio is evaluated by a quadratic polynomial approximation, which requires three calculations with different attack angles (10, 25 and 40 degrees). As for the subsonic case, it is evaluated by a cubic polynomial approximation, which requires four calculations with different attack angles (10, 25, 40 and 55 degrees). Flow conditions are summarized in Table 1.

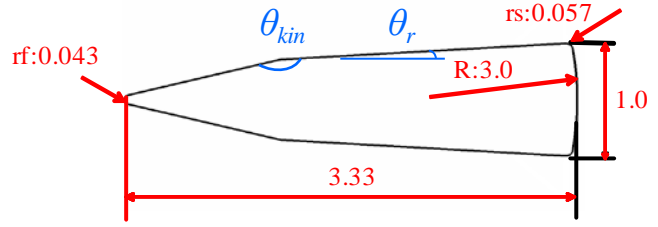


Figure 3. Body configuration

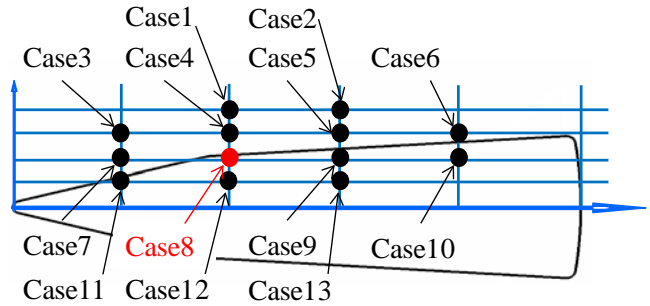


Figure 4. Exploration area

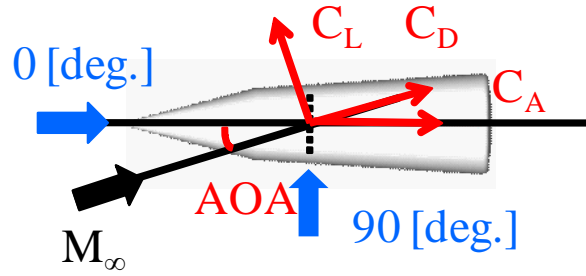


Figure 5. Definition of characteristics

Table 1. Flow conditions

	Mach number	Angle of Attack [degree]
Ascent phase	2.0	0
Return phase	2.0	10, 25, 40
	0.8	10, 25, 40, 55

III. Numerical methods

A. Flow Analysis Method

Three-dimensional Favre-averaged Navier-Stokes equations are employed as governing equations in this study. Convective terms are evaluated by the SLAU scheme which is a family of AUSM-type schemes. High-order space accuracy is obtained using the 3rd order MUSCL approach with the interpolation of primitive variables. The viscous terms are evaluated by the usual 2nd order central differencing scheme, and the eddy viscosity is modeled by the Baldwin-Lomax turbulence model³ with the Degani-Schiff's modification⁴. The CFD code applied in this work has been used in large number of practical applications for many years and the reliability of the current calculation is validated for the similar configurations².

The computational grid is O-O topology as shown in Fig. 6. The computational domain covers half of the body. The grid contains 100 points along the body surface in the flow direction from the nose to the end of the body, 53 points in circumferential direction which are equally-divided for half of the body and 93 points in the radial direction from the body surface to the computational outer boundary. The region of the computational domain is from -20.0 to +20.0 in all directions. The base area is used as the reference area to calculate the aerodynamic coefficients. The reference length is the base diameter and Reynolds number is 10^7 .

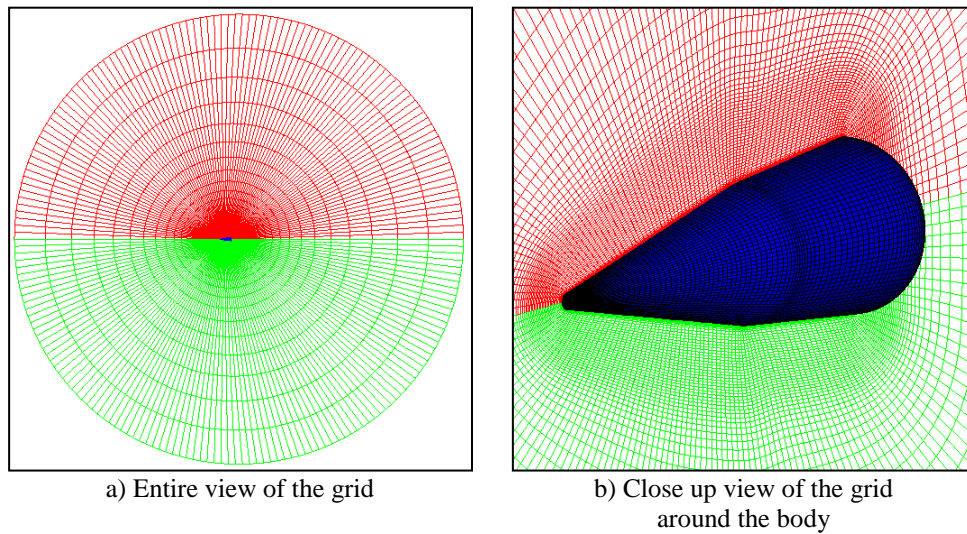


Figure 6. Computational grid

B. Verification of Computational Grid Resolution

The previous study by Fujimoto et. al.² showed the good agreement between the experimental data by NASA and the numerical results for the aerodynamic characteristics of Apollo capsule. They used a conventional numerical method and the grid of $91 \times 53 \times 61$, which are almost the same with this work. The numerical method used in this work has a certain level of the reliability for capsule geometry. However, the body configurations, discussed here have a slender shape and a kink, which are different from Apollo capsule. So, the numerical results should be compared with the experimental data but there is few experimental data in this configuration. Therefore the grid convergence check is conducted with the grid in higher resolution to confirm whether there is enough resolution in the grid used in this work. The computational grid with the higher resolution contains about 4 million points in total; 200 points along the body surface in the flow direction from the nose to the end of the body, 106 points in circumferential direction which are equally-divided for half of the body and 186 points in the radial direction from the body surface to the computational outer boundary. Regarding calculation conditions Mach number is 0.8 and attack angle is 40 degrees for the subsonic case, and Mach number is 2.0 and attack angles are 0 and 25 degrees for the supersonic case. The body configuration of Case2, 5 and 6 are used.

Fig. 7 shows C_A in the supersonic case and L/D in supersonic and subsonic case with two kinds of grids. In Fig. 7a), C_A with the fine grid is smaller than that with the coarse grid in all cases. Regarding the grid resolution, the biggest and smallest difference of C_A due to the difference of the grid resolution is 8% in Case 6 and 4% in Case 2, respectively. As for the geometry change, the difference of C_A between Case5 and Case6 is 13% in fine grid calculation and 12% in coarse grid calculation. From these results, the calculation with the coarse grid is sufficient

to evaluate the difference of C_A caused by the geometry change because the order of the magnitude of C_A is not changed by the grid resolution although the difference between the magnitude calculated by the coarse grid and that

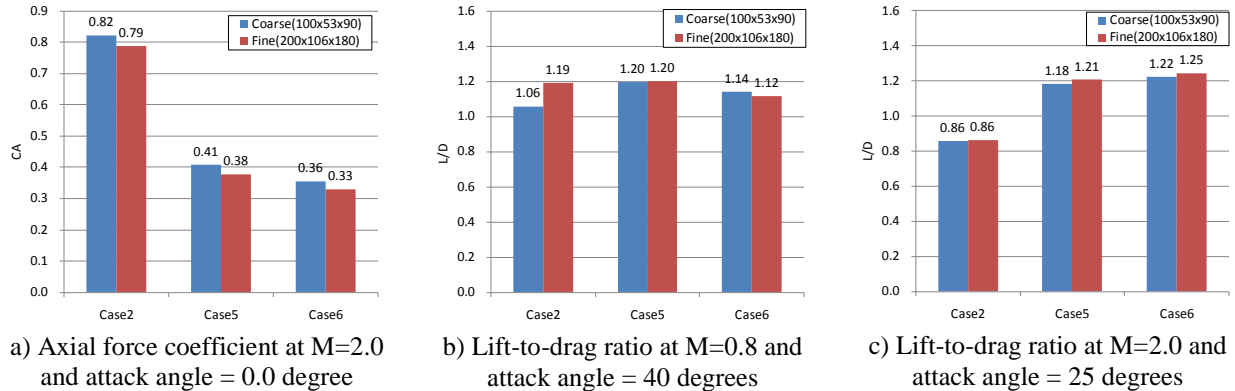
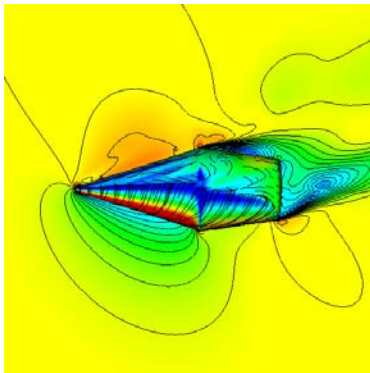
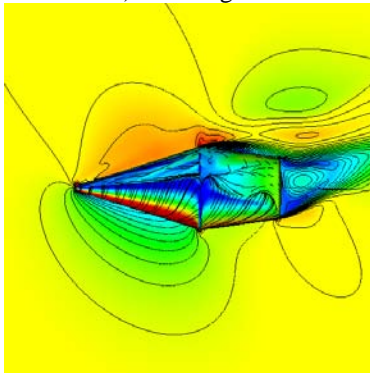


Figure 7. Grid resolution studies

of the fine grid is about 8% at a maximum. Fig. 7b) shows that the difference of L/D between the coarse grid and the fine grid is within 2% in Case5 and Case6, while 12% in Case2 for the subsonic case. It is caused mainly by the difference of separation region of the upper surface of the body after the kink. Figure 8, 9 and 10 show time averaged surface pressure distributions, stream lines and Mach number distributions for Case2, 5 and 6 at Mach number is 0.8 and attack angle is 40 degrees. The comparison between Fig. 9a) and Fig. 9b) shows little difference in the surface pressure distribution and stream lines for Case5. There is not big separation region in the rear of the kink. Case6 shown in Fig.10 is the same with the Case5. While, the comparison between Fig. 8a) and 8b) shows that the separation region of the coarse grid is bigger than that of the fine grid at upper surface after the kink for Case2.

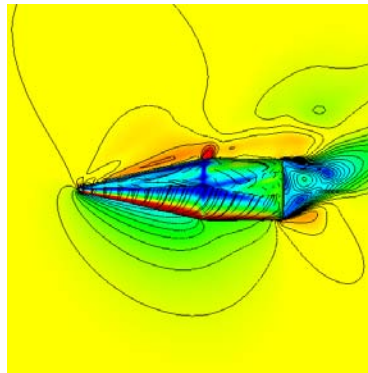


a) Coarse grid

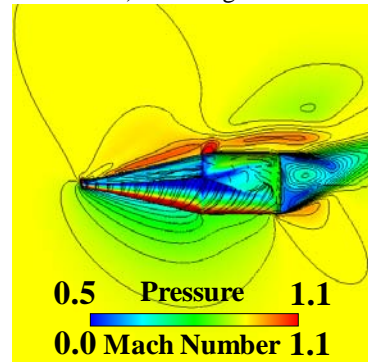


b) Fine grid

Figure 8. Flow field of Case2 at M=0.8 and attack angle = 40 degrees.

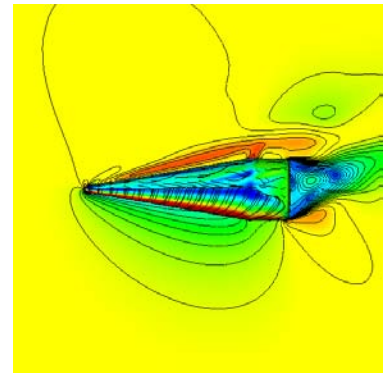


a) Coarse grid

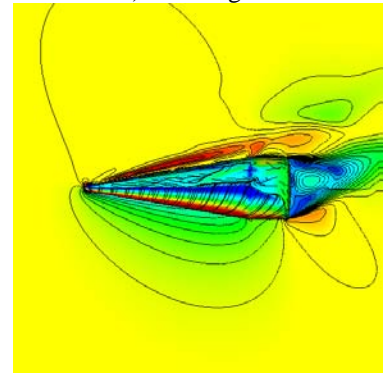


b) Fine grid

Figure 9. Flow field of Case5 at M=0.8 and attack angle = 40 degrees.



a) Coarse grid



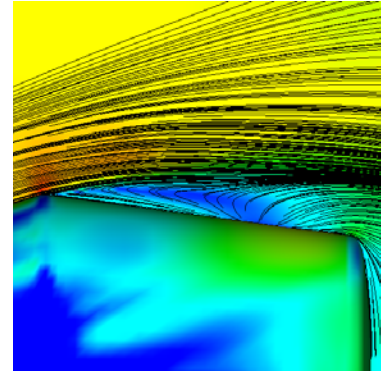
b) Fine grid

Figure 10. Flow field of Case6 at M=0.8 and attack angle = 40 degrees.

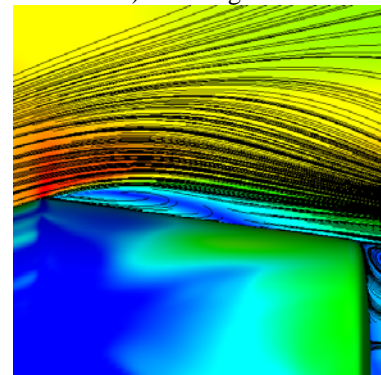
Fig. 11 shows enlarged view of the flow at the rear of the kink for Case2. Difference between the coarse grid and the fine grid can be seen at the surface pressure distributions. The low pressure area of the fine grid is larger than that of the coarse grid. From the comparison of stream lines, the separation region has a difference. The separated flows are reattached in the fine grid case, while not in the coarse grid case. Therefore, the coarse grid of Case2 shows lower lift-to-drag ratio than the fine grid due to the increase of the pressure on the upper surface after the kink, which is caused by the large separation. Thus, the difference of the lift-to-drag ratio in Case2 is larger than that in the other cases because the flow on the upper surface after the kink is different between the coarse grid and the fine grid. Special cares are required when the diameter of the kink exceeds the base diameter and relatively larger separation is occurred in downstream of the kink. However, calculations using the coarse grid could evaluate lift-to-drag ratio in subsonic case except for the configurations like Case2 mentioned above.

Fig. 7c) shows that the lift-to-drag ratios are almost the same in every coarse and fine grid. The biggest difference is within 3% in Case5. Thus, the lift-to-drag ratio in supersonic case can be evaluated accurately using the coarse grid.

Verification about the grid resolution is summarized as follows. The numerical method used in this work with 0.5 million grid points can predict C_A in supersonic flight and the lift-to-drag ratio in both supersonic and subsonic flights with sufficient accuracy, which is required in the conceptual design stage. However it is insufficient to calculate the body configuration as Case2, whose kink diameter exceeds the base diameter. So design exploration should be done only for body configurations whose kink diameter doesn't exceed the base diameter.



a) Coarse grid



b) Fine grid

Figure 11. Enlarged view of the flow field at the rear of the kink for Case2.

C. Evaluation of Maximum Lift-to-drag Ratio

The maximum lift-to-drag ratio is evaluated by a quadratic polynomial approximation, which requires three calculations with different attack angles for the supersonic flight and by a least squares method with four calculations with different attack angles for the subsonic flight because the attack angle of the maximum lift-to-drag ratio cannot be known in advance. It is ideal to conduct many calculations with different attack angles for one configuration in order to evaluate the maximum lift-to-drag ratio accurately. However, it is computationally expensive and not suitable for the current work, which requires many calculations for various configurations. Therefore, these approximations are adopted to reduce the calculation cost. Figure 12 shows the results at 2.0 of Mach number and at 0, 25 and 40 degrees of attack angles in Case3, 4, 5 and 6. Similarly, Figure 13 shows the results at 0.8 of Mach number and at 10, 25, 40 and 55 degrees of attack angles in Case3, 4, 5 and 6, respectively. From these figures, it is confirmed that the attack angle of maximum lift-to-drag ratio lies within the region of the calculated attack angles. Therefore, the maximum lift-to-drag ratios for all configurations are calculated by the approximation with the lift-to-drag ratios calculated by different attack angles.

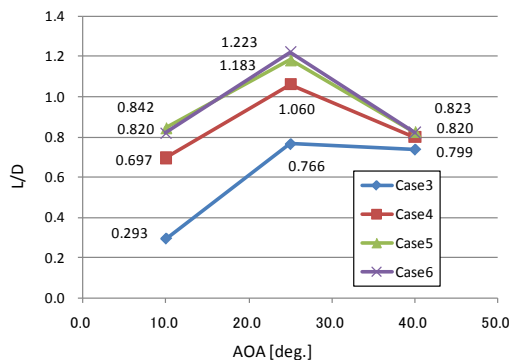


Figure 12. Lift-to-drag ratio at M=2.0

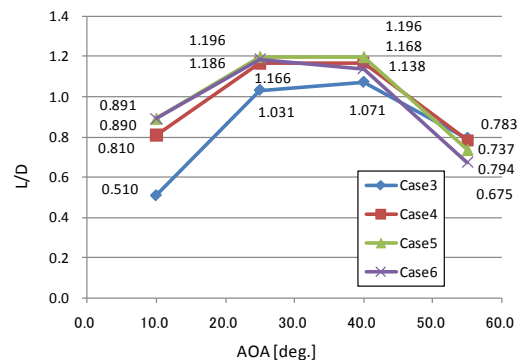


Figure 13. Lift-to-drag ratio at M=0.8

Validation is conducted if the maximum lift-to-drag ratio calculated by the approximation is correct. The maximum lift-to-drag ratio is calculated for the configurations of Case3 and 5 at the attack angle given by the approximation methods in both supersonic and subsonic cases. The calculated maximum lift-to-drag ratios for Case3 and 5 are 0.81 and 1.19 in supersonic case, and 1.13 and 1.28 in subsonic case, respectively. The difference is less than 1% in supersonic case and around 3% in subsonic case, showing the good agreement between calculated and approximated values. Thus, this approximation method is sufficient to evaluate the maximum lift-to-drag ratio.

IV. Results and Discussions

A. Flow Fields

Supersonic flow during the launch

Figure 14 shows the pressure distributions on the body surface and Mach number distributions on the symmetric plane of the time-averaged flow fields during the launch. Mach number is 2.0 and attack angle is 0 degree. Figure 14a) and 14b) show flow fields around two typical low drag configurations. Figure 14c) and 14d) show flow fields around two typical high drag configurations. The high drag configuration have larger semi-apex angle at front body than low drag configurations. It has a shock wave in front of the body, which has a deeper angle against the free stream. It increases the wave drag and in consequence the total drag is increased. While, the shock wave of the low drag configuration has shallow angle against the free stream. It makes wave drag decreased and then the total drag decreased.

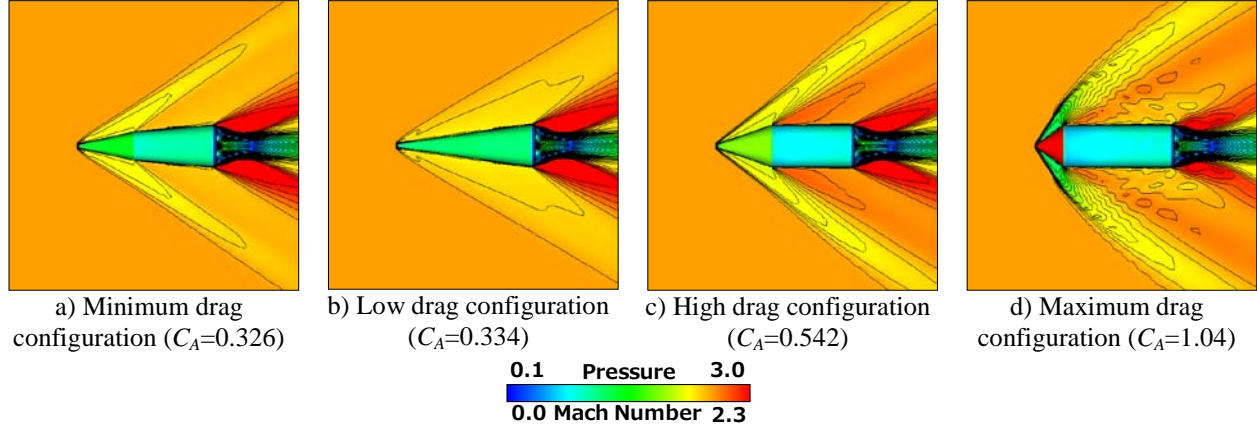


Figure 14. Distributions of surface pressure and space Mach number at $M=2.0$ and attack angle = 0 degrees (supersonic flight during the launch)

Supersonic flow during the return

Figure 15 shows the pressure distributions, streamlines on the body surface and Mach number distributions on the symmetric plane of the time-averaged flow fields in the supersonic flight during the return phase. Since the maximum lift-to-drag ratios are obtained at 25 degrees of the attack angle for all configurations, the flow fields at that attack angle are shown. Figure 15a) and 15b) show the flow fields around two typical configurations which have high lift-to-drag ratio. Figure 15c) and 15d) show the flow fields around two typical configurations which have low lift-to-drag ratio. The configurations having high lift-to-drag ratio are similar to conical shape. While, configurations having low lift-to-drag ratio have larger semi-apex angle of the fore body. By comparing configurations having high lift-to-drag ratio with low lift-to-drag ratio, the shock wave in front of the body becomes stronger as to the increase of the semi-apex angle of the fore body, increasing the wave drag and decreasing the lift-to-drag ratio.

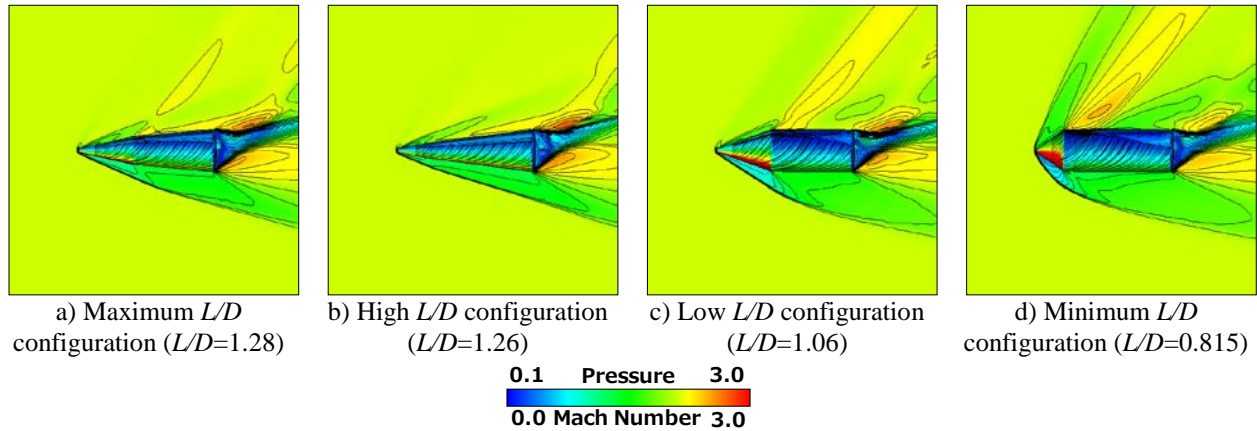


Figure 15. Distributions of surface pressure and space Mach number at $M=2.0$ and attack angle=25 degrees (supersonic flight during the return)

Subsonic flow during the return

Figure 16 shows the pressure distributions, streamlines on the surface and Mach number distributions on the symmetric plane of the time-averaged flow fields in subsonic flight during the return phase. Attack angle of the flow fields are 25 degrees. Figure 16a) and 16b) show the flow fields around two typical configurations having high lift-to-drag ratio. Figure 16c) and 16d) show the flow fields around two typical configurations having low lift-to-drag ratio. The configurations having high lift-to-drag ratio have larger semi-apex angle of fore body. While, configurations having low lift-to-drag ratio are more conical in shape. This result is opposite to the supersonic case. As wave drag has strong effect in the supersonic case, it is necessary to make the wave drag smaller in order to make the lift-to-drag ratio larger. While, as wave drag has small effect in the subsonic case, other factors like non linear effects make the lift-to-drag ratio larger. Thus following two configurations are contradicted each other. One is configurations which decrease aerodynamic drag in supersonic flight of the launch phase and increase the lift-to-drag ratio in supersonic flight of the return phase. The other is configurations which increase lift-to-drag ratio in subsonic flight of the return phase.

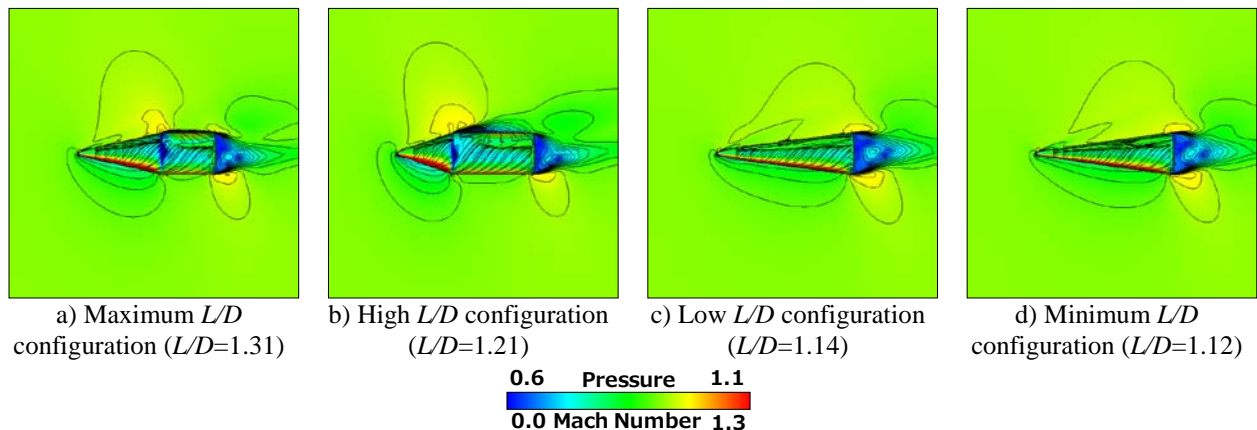


Figure 16. Distributions of surface pressure and space Mach number at $M=0.8$ and attack angle=25 degrees (subsonic flight during the return)

B. Design Exploration

All calculated results are shown in following figures. Figure 17 shows the correlation between the aerodynamic drag during the ascent phase and the maximum lift-to-drag ratio during the supersonic flight of the return phase. The positive correlation between them can be seen, suggesting an existence of the configuration which realizes two objectives at the same time, minimization of the drag and maximization of the maximum lift-to-drag ratio. This is because the configuration with a small semi-apex angle of the fore body can decrease the wave drag in supersonic flight, reducing the aerodynamic drag and increasing the lift-to-drag ratio. Figure 18 shows the correlation between

the aerodynamic drag during the ascent phase and the maximum lift-to-drag ratio during the subsonic flight of the return phase. There is a trade-off between two objectives; the minimization of the drag and the maximization of the maximum lift-to-drag ratio, especially around the desirable region. Figure 19 shows the correlation between the maximum lift-to-drag ratio during the supersonic and subsonic flight of the return phase. There also exists a trade-off around the desirable region. As for the maximum lift-to-drag ratio, the geometry which maximizes the maximum lift-to-drag ratio in the supersonic flight is similar to the conical geometry. However, the geometry which maximizes the maximum lift-to-drag ratio in subsonic flight is not conical but like a combined circular cone and cylinder.

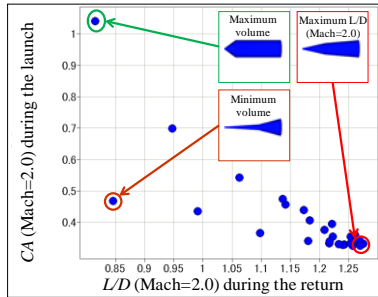


Figure 17. Correlation between the aerodynamic drag (C_A) during the launch and the lift-to-drag-ratio (L/D) during the supersonic return flight.

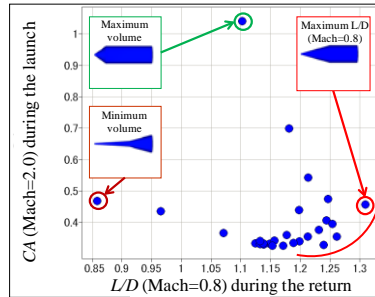


Figure 18. Correlation between the aerodynamic drag (C_A) during the launch and the lift-to-drag-ratio (L/D) during the subsonic flight.

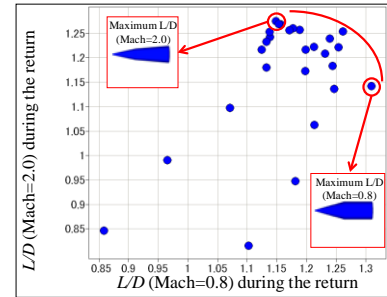


Figure 19. Correlation between the lift-to-drag-ratio (L/D) in the supersonic flight and that in the subsonic flight.

Figure 20, 21 and 22 show the correlation of the body volume with the aerodynamic drag during the ascent phase, the maximum lift-to-drag ratio during the supersonic flight of the return phase and the maximum lift-to-drag ratio during the subsonic flight of the return phase, respectively. The body volume is non-dimensionalized by the body volume of the conical geometry. The aerodynamic drag and the maximum lift-to-drag ratio have an extreme value according to the change of the body volume. Therefore the body volume has a weak trade-off with these aerodynamic characteristics.

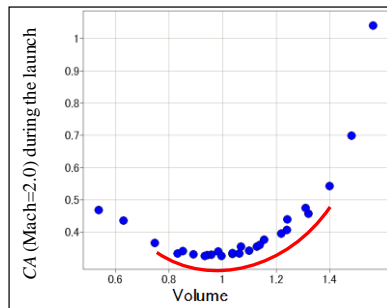


Figure 20. Correlation between the aerodynamic drag (C_A) during the launch and the body volume.

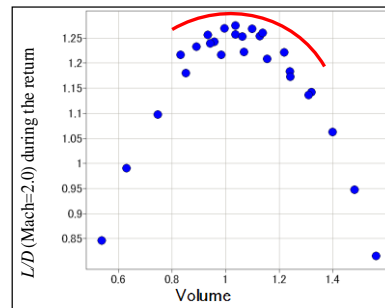


Figure 21. Correlation between the lift-to-drag ratio (L/D) in the supersonic flight and the body volume.

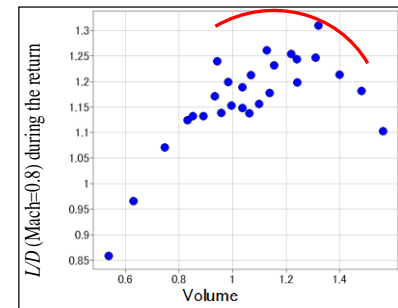


Figure 22. Correlation between the lift-to-drag ratio (L/D) in the subsonic flight and the body volume.

Correlation between objective functions and design variables

Figure 23 shows the correlation of the aerodynamic drag during the ascent with the kink angle θ_{kin} and the aft body angle θ_r , respectively. These figures also show the typical body configurations and their body volume. The aerodynamic drag during the ascent has a stronger correlation with the kink angle θ_{kin} than the aft body angle θ_r . The body configuration with the minimum drag is not without the kink ($\theta_{kin} = 180$ degrees), but with the kink, whose angles are about 175 degrees and 165 degrees. There are two groups for the minimum drag configurations. One is the group where the kink is located near the tip of the nose with 165 degrees of the kink angle θ_{kin} , and the other is the group where the kink is located in the posterior part of the nose with 175 degrees of the kink angle θ_{kin} . Comparing these two groups, the configuration with 165 degrees of the kink angle θ_{kin} is better because the body volume of the configuration is 1.28 which is larger than 1.12 of the configuration with 175 degrees of the kink angle

θ_{kin} . This result is different from the common idea that the conical geometry has the minimum drag. It is worth for further studies.

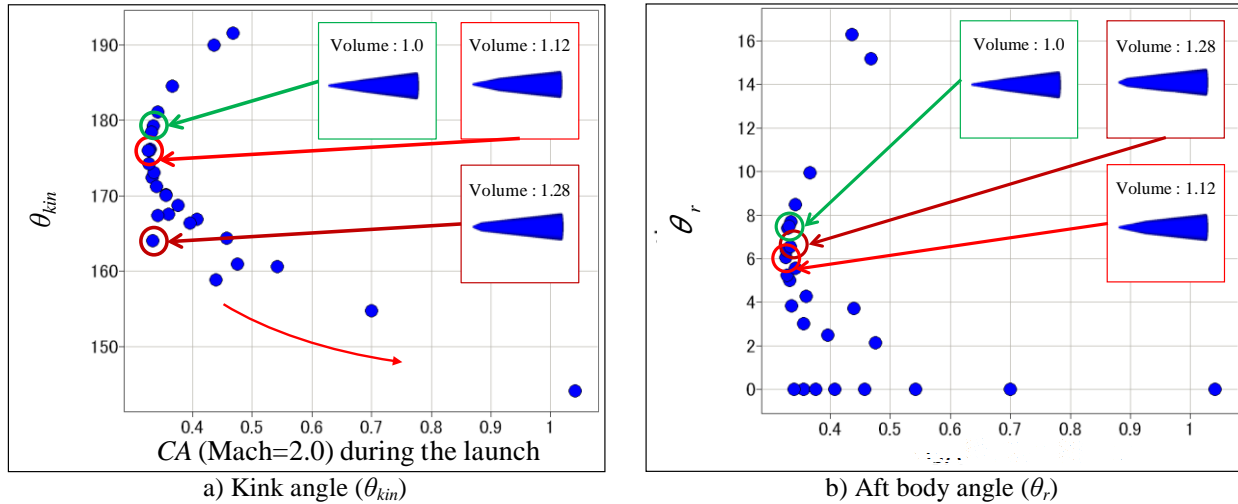


Figure 23. Correlation between the aerodynamic drag (C_A) during the supersonic flight of the launch and the design variables (θ_{kin} and θ_r)

Figure 24 shows the correlation of the maximum lift-to-drag ratio during the supersonic return flight with the kink angle θ_{kin} and the aft body angle θ_r , respectively. Regarding the kink angle θ_{kin} , the maximum lift-to-drag ratio is maximized around 172 degrees of the kink angle θ_{kin} . The variation of the values can be seen at that maximum area. As for the aft body angle θ_r , it maximized around 5 degrees. It also has the variation at the maximum area. Figure 24 also shows the body volume for two configurations which have maximum lift-to-drag ratio. Even having the same maximum lift-to-drag ratio, these two body configurations show different body volume as 1.20 and 1.57, whose difference is 30%.

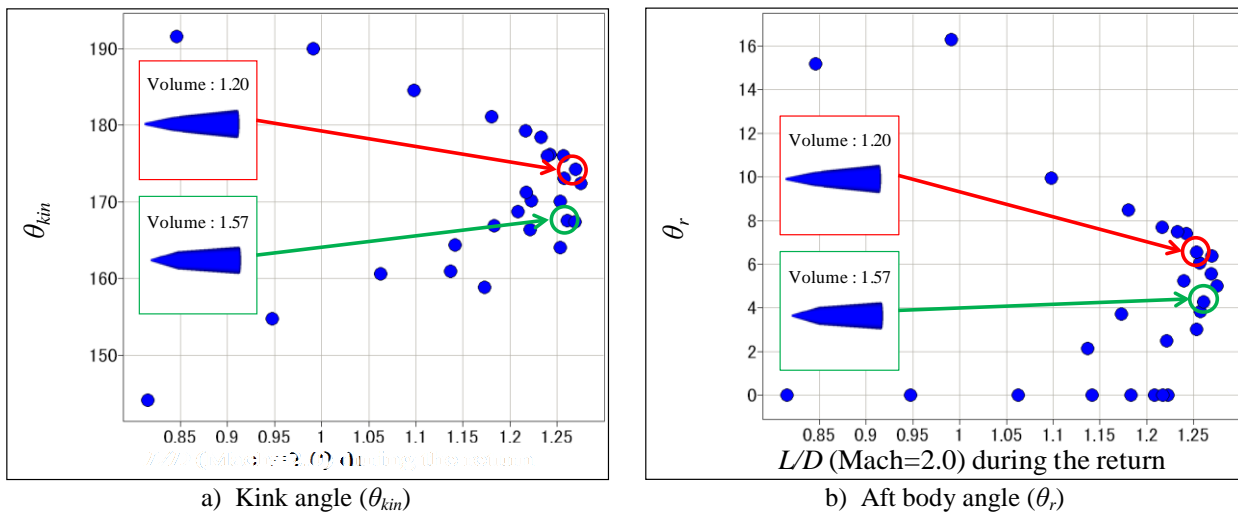


Figure 24. Correlation between the lift-to-drag ratio (L/D) during the supersonic flight of the return phase and the design variables (θ_{kin} and θ_r)

Figure 25 shows the correlation of the maximum lift-to-drag ratio during the subsonic return flight with the kink angle θ_{kin} and the angle of the aft body θ_r , respectively. Regarding the kink angle θ_{kin} , the maximum lift-to-drag ratio is maximized around 165 degrees of the kink angle θ_{kin} . The variation of the maximum lift-to-drag ratio around the maximized area is larger than that in the supersonic flight of the return phase. As for the aft body angle θ_r , the trend is relatively simple. The maximum lift-to-drag ratio becomes larger as to the decrease of the aft body angle θ_r , becoming maximum around 0 degree. However, as the maximum lift-to-drag ratio has large variance around 0 degree, 0 degree of the aft body angle θ_r does not always ensure the maximization of the maximum lift-to-drag ratio.

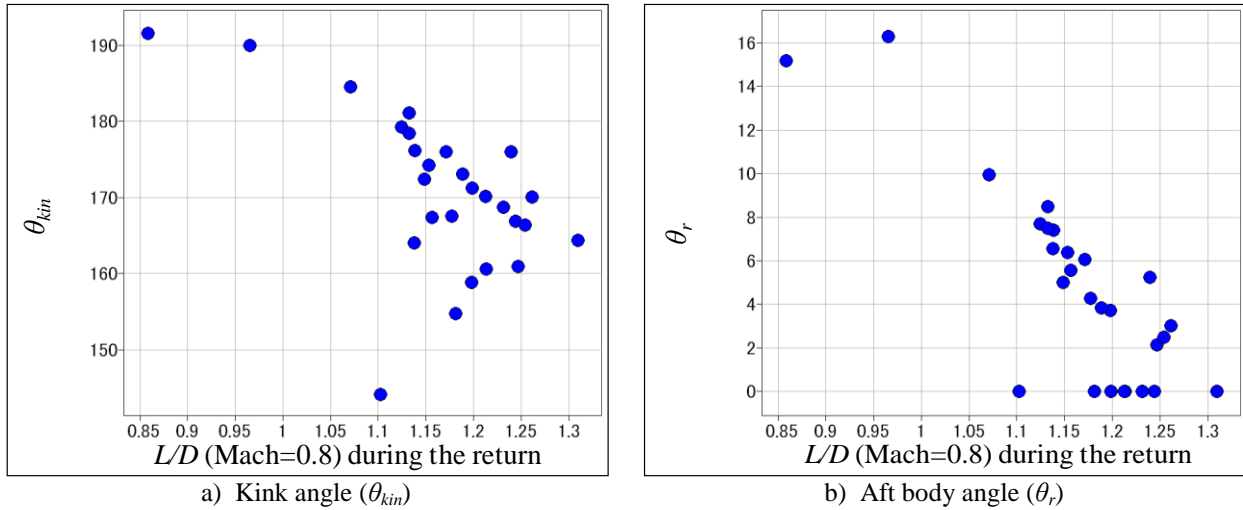


Figure 25. Correlation between the lift-to-drag ratio (L/D) during the subsonic flight of the return phase and the design variables (θ_{kin} and θ_r)

V. Conclusions

Multi-objective design exploration of the aerodynamic configurations is conducted for the vertical landing rocket vehicle by using CFD in order to minimize the aerodynamic drag during the ascent phase, to maximize the maximum lift-to-drag ratio during the return phase and to maximize the body volume. CFD analysis with 0.5 million grid points can precisely predict the difference of the aerodynamic drag and the maximum lift-to-drag ratio according to the difference of the body configuration except for configurations whose diameter of the kink exceeds the base diameter. Following aerodynamic design information required in the conceptual design stage are obtained about the correlation between the objectives and between the objectives and the design variables.

- ✓ The minimization of the aerodynamic drag during the ascent phase is positively correlated with the maximization of the maximum lift-to-drag ratio during the supersonic flight of the return phase.
- ✓ There is a trade-off around the optimized solutions between the minimization of the aerodynamic drag during the ascent phase and the maximization of the maximum lift-to-drag ratio during the subsonic flight of the return phase.
- ✓ The aerodynamic drag and the lift-to-drag ratio have the extreme value to the body volume.
- ✓ The minimization of the aerodynamic drag during the ascent phase has a strong correlation with the kink angle θ_{kin} . The body configuration of the minimum drag is different from the conical geometry which has no kink.
- ✓ The maximization of the maximum lift-to-drag ratio during the supersonic flight of the return phase is achieved when the design variables θ_r is about 5 degrees and θ_{kin} is about 172 degrees. However, this maximum point doesn't always ensure the maximization of the lift-to-drag ratio.
- ✓ The maximization of the maximum lift-to-drag ratio during the subsonic flight of the return phase is achieved when the design variables θ_r is almost 0 degrees and θ_{kin} is about 165 degrees. However, this maximum point doesn't always ensure the maximization of the lift-to-drag ratio and the variance is larger than that of the supersonic flight.

References

- ¹ Nonaka, S., Ogawa, H. and Inatani, Y., "Aerodynamic Design Considerations in Vertical Landing Rocket Vehicle", AIAA Paper 01-1898, 2001.
- ² Fujimoto, K., Fujii, K. and Tsuboi, N., "Compressible Flow Simulations over Basic Reusable Rocket Configurations," Symposium on Applications in Computational Fluid Dynamics ASME/JSME Joint Fluids Engineering Division, 2003.
- ³ Baldwin, B. and Lomax, H., "Thin Layer Approximation and Algebraic Model for Separated Turbulent Flows," AIAA Paper 78-257, Jan., 1978.
- ⁴ Degani, D. and Schiff, L.B., "Computation of Turbulent Supersonic Flows around Pointed Bodies Having Crossflow Separation," *Journal of Computational Physics*, 66,173-196(1986).